

LETTER TO THE EDITOR

Water abundance variations around high-mass protostars: HIFI observations of the DR21 region[★]

F.F.S. van der Tak^{1,2}, M.G. Marseille¹, F. Herpin³, F. Wyrowski⁴, A. Baudry³, S. Bontemps³, J. Braine³, S. Doty¹³, W. Frieswijk², G. Melnick¹², R. Shipman¹, E.F. van Dishoeck^{5,14}, A.O. Benz⁹, P. Caselli¹⁵, M. Hogerheijde⁵, D. Johnstone^{16,17}, R. Liseau⁸, R. Bachiller¹⁸, M. Benedettini¹⁹, E. Bergin²⁰, P. Bjerkeli⁸, G. Blake²¹, S. Bruderer⁹, J. Cernicharo²², C. Codella¹⁹, F. Daniel^{31,22}, A.M. di Giorgio¹⁹, C. Dominik²³, P. Encrenaz²⁴, M. Fich²⁵, A. Fuente¹⁸, T. Giannini¹⁹, J. Goicoechea²², Th. de Graauw¹⁰, F. Helmich¹, G. Herczeg¹⁴, J. Jørgensen²⁶, L. Kristensen⁵, B. Larsson²⁷, D. Lis²¹, C. McCoe²⁵, D. Neufeld²⁸, B. Nisini¹⁹, M. Olberg⁸, B. Parise^{4,6}, J. Pearson²⁹, R. Plume³⁰, C. Risacher¹, J. Santiago¹⁸, P. Saraceno¹⁹, M. Tafalla¹⁸, T. van Kempen¹², R. Visser⁵, S. Wampfler⁹, U. Yıldız⁵, L. Ravera⁷, P. Roelfsema¹, O. Siebertz⁶, and D. Teyssier¹¹

(Affiliations can be found after the references)

Received 26 March 2010 ; accepted 20 April 2010

ABSTRACT

Context. Water is a key molecule in the star formation process, but its spatial distribution in star-forming regions is not well known.

Aims. We study the distribution of dust continuum and H₂O and ¹³CO line emission in DR21, a luminous star-forming region with a powerful outflow and a compact H II region.

Methods. *Herschel*-HIFI spectra near 1100 GHz show narrow ¹³CO 10–9 emission and H₂O 1₁₁ – 0₀₀ absorption from the dense core and broad emission from the outflow in both lines. The H₂O line also shows absorption by a foreground cloud known from ground-based observations of low-*J* CO lines.

Results. The dust continuum emission is extended over 36'' FWHM, while the ¹³CO and H₂O lines are confined to ≈24'' or less. The foreground absorption appears to peak further North than the other components. Radiative transfer models indicate very low abundances of ~2×10⁻¹⁰ for H₂O and ~8×10⁻⁷ for ¹³CO in the dense core, and higher H₂O abundances of ~4×10⁻⁹ in the foreground cloud and ~7×10⁻⁷ in the outflow.

Conclusions. The high H₂O abundance in the warm outflow is probably due to the evaporation of water-rich icy grain mantles, while the H₂O abundance is kept down by freeze-out in the dense core and by photodissociation in the foreground cloud.

Key words. ISM: molecules – Stars: formation – astrochemistry – ISM: individual objects: DR21

1. Introduction

The water molecule is a key species throughout the formation of stars and planets. In the gas phase, it acts as a coolant of collapsing interstellar clouds; in the solid state, it acts as glue for dust grains in protoplanetary disks to make planetesimals; and as a liquid, it acts as transporter bringing molecules together on planetary surfaces, a key step towards biogenic activity. The first role is especially important for high-mass star formation which depends on the balance between the collapse of a massive gas cloud and its fragmentation (Zinnecker & Yorke 2007).

Interstellar H₂O is well known from ground-based observations of the 22 GHz maser line. Previous space-based submm and far-IR observations have measured H₂O abundances ranging from 10⁻⁸ in cold gas to 10⁻⁴ in warm gas (ISO: Van Dishoeck & Helmich 1996; SWAS: Melnick & Bergin 2005; Odin: Bjerkeli et al. 2009) but did not have sufficient angular resolution to determine the spatial distribution of H₂O. In contrast, space-based mid-IR and ground-based mm-wave observations have high angular resolution but

only probe the small fraction of the gas at high temperatures (Van der Tak et al. 2006; Watson et al. 2007).

This paper presents observations of an H₂O ground state line at >3× higher angular resolution than previously possible for such lines. Through radiative transfer models, we compare the abundance distribution of H₂O with that of ¹³CO and dust. The source DR21 (Main) is a high-mass protostellar object (*L*=45,000 *L*_⊙) located in the Cygnus X region at *d*=1.7 kpc (Schneider et al. 2006), about 3' South of the well-known DR21(OH) object (also known as W75S). Maps of the 1.2 mm dust emission show a dense core with a mass of 600–1000 *M*_⊙ and a size of 0.19×0.14 pc FWHM, surrounded by an extended envelope with mass 4750 *M*_⊙ and size 0.3 pc (Motte et al. 2007). Gas densities of 10⁵–10⁶ cm⁻³ are derived from both the mm-wave continuum and HCN and HCO⁺ line emission (Kirby 2009). Signs of active high-mass star formation are the bright mid-IR emission (272 Jy at 21 μm), the presence of an H₂O 22 GHz maser (see catalog of Braz & Epchtein 1983) and emission from ionized gas extending over 20–30'' (Roelfsema et al. 1989). Together with the powerful molecular outflow (Garden et al. 1991) these signs indicate that the source is relatively evolved within the embedded phase of high-mass star formation, beyond the ‘ultracompact H II region’ phase.

[★] *Herschel* is an ESA space observatory with science instruments provided by European-led Principal Investigator consortia and with important participation from NASA

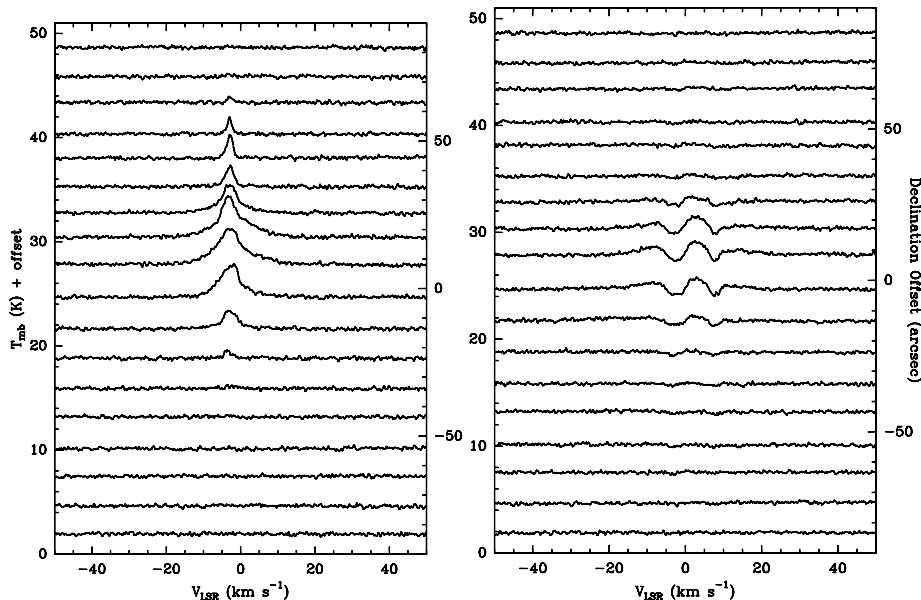


Fig. 1. Spectra of ^{13}CO 10 – 9 (left) and H_2O $1_{11} - 0_{00}$ (right) lines toward DR21, taken with the WBS backend.

2. Observations

The DR21 region was observed with the Heterodyne Instrument for the Far-Infrared (HIFI; De Graauw et al, this volume) on-board ESA’s *Herschel* Space Observatory (Pilbratt et al, this volume) on June 22, 2009. Spectra were taken in double sideband mode using receiver band 4b, with $\nu_{\text{LO}}=1107.990$ GHz and $\nu_{\text{IF}}=6$ GHz. The data were taken during the performance verification (PV) phase using the double beam switch observing mode with a throw of 2.5 to the SW. The position observed is R.A. 20:39:02.38, Dec +42:19:33.5 (J2000), close to radio peak C from Roelfsema et al. (1989). A strip map was made in the N-S direction, spanning offsets from +90'' to –90'' at a 10.5 spacing, half the beam size of 21'' FWHM at our observing frequency, which corresponds to 0.17 pc at the distance of DR21. This beam size was measured before launch and is 10% larger than the diffraction limit due to spillover effects.

Data were taken with two backends: the acousto-optical Wide-Band Spectrometer (WBS) which covers 1140 MHz bandwidth at 1.1 MHz (0.30 km s^{-1}) resolution, and the correlator-based High-Resolution Spectrometer (HRS), which covers 230 MHz bandwidth at 0.48 MHz (0.13 km s^{-1}) resolution. Two polarizations are available except for the HRS data of H_2O .

The system temperature of our data is 340–360 K DSB and the integration time is 67 seconds per position (ON+OFF). Calibration of the raw data onto T_A^* scale was performed by the in-orbit system (Roelfsema et al, in prep); conversion to T_{mb} was done assuming a beam efficiency of 0.67 as estimated by the Ruze formula and validated by raster maps of Saturn (M. Olberg, priv. comm.). Currently, the flux scale is accurate to $\approx 10\%$ which will improve when the telescope efficiency and sideband ratio are measured on Mars. The calibration of the data was performed in the *Herschel* Interactive Processing Environment (HIPE; Ott 2010) version 2.1; further analysis was done within the CLASS¹ package. After inspection, data from the two polarizations were averaged together to obtain rms noise levels of 97 mK on 0.5 MHz channels for the WBS data, 195 mK on 0.24 MHz channels for the ^{13}CO HRS data and 244 mK on 0.24 MHz channels for the H_2O HRS data.

3. Results

Figure 1 shows the WBS spectra from both receiver sidebands at each of the 18 offset positions. The spectra from both backends show a continuum signal and two line features. The first line feature is seen in emission at $\nu = 1101.357$ GHz LSB or 1114.623 GHz USB, which we identify with the ^{13}CO $J=10 \rightarrow 9$ line at 1101.349597 GHz². This line has an upper level energy (E_u) of 291 K and a critical density of $1 \times 10^6 \text{ cm}^{-3}$, using collision data from Flower (2001). The second feature has a mixed emission-absorption profile and lies at $\nu = 1102.423$ GHz LSB or 1113.557 GHz USB, which we identify with the H_2O $J_{K_p K_o}=1_{11} \rightarrow 0_{00}$ line at 1113.34306 GHz. This line has $E_u = 53$ K and a critical density of $3\text{--}6 \times 10^8 \text{ cm}^{-3}$, using collision data from Faure et al. (2007). No other lines are detected.

Figure 2 shows the HRS spectra of the ^{13}CO and H_2O lines at the central position, with the continuum subtracted. The ^{13}CO line profile has a double structure which is seen to be well reproduced by the sum of two Gaussians: a narrow component ($\Delta V=4.9 \text{ km s}^{-1}$) centered at $V_{\text{LSR}}=-3.2 \text{ km s}^{-1}$, which we attribute to the molecular cloud core (protostellar envelope), and a broad component ($\Delta V=15.2 \text{ km s}^{-1}$) centered at $V_{\text{LSR}}=-2.0 \text{ km s}^{-1}$, which we ascribe to the molecular outflow. In contrast, the H_2O line profile shows two absorption features, with strong emission in between, and weaker emission on the far blue- and redshifted sides. Overplotted is a decomposition with three Gaussian components: broad ($\Delta V=23.8 \text{ km s}^{-1}$) emission centered at $V_{\text{LSR}}=-1.0 \text{ km s}^{-1}$, and absorptions at $V_{\text{LSR}}=-2.6 \text{ km s}^{-1}$ and $+7.6 \text{ km s}^{-1}$ with $\Delta V=5.0$ and 3.0 km s^{-1} . This shape resembles the prediction by Poelman & van der Tak (2007) for the H_2O ground state lines towards high-mass protostellar envelopes for the case of a constant, low $\text{H}_2\text{O}/\text{H}_2 \sim 10^{-9}$ with two modifications. First is the broad emission also seen in ^{13}CO which is likely due to the outflow. Second is the absorption at $V_{\text{LSR}}=7.6 \text{ km s}^{-1}$ which is known from ground-based observations of low- J CO lines (Jakob et al. 2007) and likely due to a foreground cloud. This absorption is not seen in the ^{13}CO 10-9 line, nor in ground-based observations of mid- J HCN and

¹ <http://www.iram.fr/IRAMFR/GILDAS>

² Spectroscopic data are taken from the CDMS catalog (Müller et al. 2005) at <http://cdms.de>

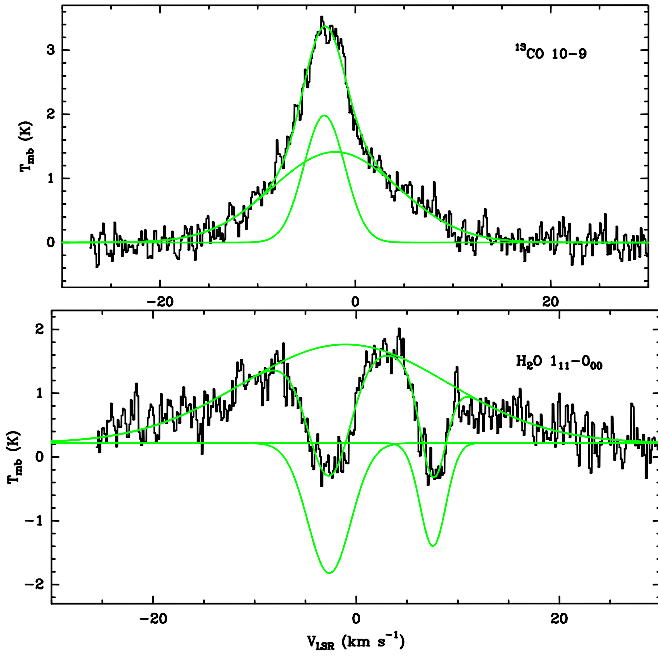


Fig. 2. Spectra of ^{13}CO 10 – 9 (top) and H_2O 1₁₁ – 0₀₀ (bottom) lines toward the central position, taken with the HRS backend, with Gaussian decompositions overplotted.

HCO^+ lines, which indicates a low temperature (~ 10 K) and density ($\lesssim 10^4 \text{ cm}^{-3}$) for the foreground cloud. Both absorptions are also seen in the SWAS spectra of the o- H_2O and C^0 ground-state lines, but not in ^{13}CO 5 – 4 (Ashby et al. 2000).

Figure 3 shows the spatial brightness distribution of the continuum and the lines. The points are the results of Gaussian profile fits for the lines, and of linear baseline fits for the continuum, at each offset position. For the H_2O line, separate fits were made for the emission and the two absorption components. The curves in Figure 3 are Gaussian fits to the observed spatial distribution. The dust emission peaks at an offset of $(8.7 \pm 0.5)''$ North of the nominal position, and the emission distribution has an FWHM width of $(35.7 \pm 0.5)''$, consistent with ground-based measurements at longer wavelengths (Gibb et al. 2005; Motte et al. 2007). The peak of the ^{13}CO emission is at offset $(9.65 \pm 0.5)''$, consistent with the dust peak within the combined error, but the FWHM of the ^{13}CO emission is $(24.1 \pm 0.4)''$, essentially unresolved. The H_2O emission component has an FWHM of $(25.2 \pm 2.5)''$, similar to ^{13}CO , but its peak is shifted further South, at offset $(6.4 \pm 1.1)''$. The spatial distribution of the H_2O absorption at $V = -3 \text{ km s}^{-1}$ is the same as that of the H_2O emission, peaking at offset $(6.7 \pm 1.6)''$ with an FWHM of $(26.2 \pm 3.3)''$. In contrast, the H_2O absorption at $V = +7.5 \text{ km s}^{-1}$ peaks much further North, at offset $(14.2 \pm 1.9)''$, and is possibly extended with an FWHM of $(32.8 \pm 4.7)''$, which is a lower limit to its full width because of insufficient background signal. Indeed, Schneider et al. (2006) find that the W75N cloud extends over several arcminutes.

4. Discussion and Conclusions

To estimate the H_2O and ^{13}CO abundances from our data, we have run spherical radiative transfer models following Marseille et al. (2008). First, the dust continuum emission was modeled with the MC3D program (Wolf & Henning 2000) with the source size and luminosity kept fixed at the values in §1. The

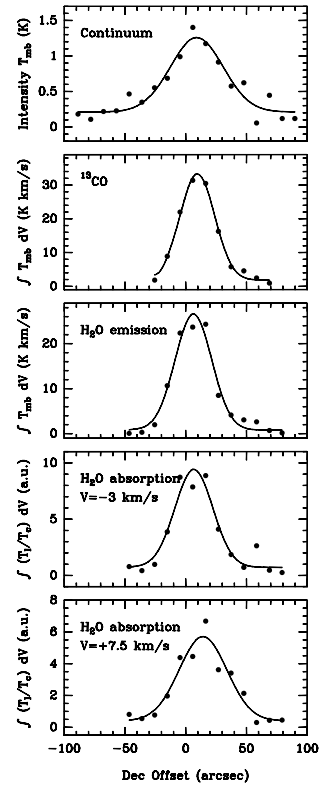


Fig. 3. Plots of observed intensity versus spatial offset with Gaussian models superposed.

continuum data are consistent with a power-law density profile $n = n_0(r/r_0)^{-\alpha}$ with the index $\alpha = 1.5$ as expected for evolved protostellar envelopes (Van der Tak et al. 2000). Derived temperatures range from 117 K at the adopted inner radius of 0.01 pc to 23 K at the outer radius of 0.3 pc; densities drop from $3 \times 10^7 \text{ cm}^{-3}$ to $2 \times 10^5 \text{ cm}^{-3}$. This temperature and density profile was adopted for the line radiative transfer with the RATRAN program (Hogerheijde & van der Tak 2000). The abundance of H_2O was varied between 10^{-10} and 10^{-7} and the ^{13}CO abundance between 10^{-7} and 10^{-6} , both independent of radius.

The red lines in Figure 4 show the results of our best-fit model. The fit to the line profiles at the central few positions is good if two components are added to the dense core model: one representing the outflow and one for the foreground cloud. This simple addition procedure is valid because the foreground cloud is transparent and the outflow is seen at an angle, so that neither component blocks the view of the dense core. The modeled optical depths are 2.8 for the H_2O line and 0.77 for ^{13}CO , and the derived abundances are uncertain to $\approx 35\%$ which is the quadratic sum of 30% from the line intensity and 20% from the core mass estimate. The model underproduces the observed line strengths at large position offsets, which suggests that the density profile flattens out at large radii, as also indicated by the observed continuum brightness at the offset positions.

Deriving the ^{13}CO and H_2O abundances in the outflow and the foreground using radiative transfer models is not possible because the masses and H_2 column densities of these components are unknown. Instead we have used RADEX (Van der Tak et al. 2007) to estimate their ^{13}CO and H_2O column densities, and use a $^{12}\text{C}/^{13}\text{C}$ ratio of 60 (Milam et al. 2005) and a CO abundance of 2×10^{-4} (Lacy et al. 1994) to convert $N(^{13}\text{CO})$ to $N(\text{H}_2)$ and estimate $x(\text{H}_2\text{O})$ as $N(\text{H}_2\text{O})/N(\text{H}_2)$. For the foreground cloud, we adopt $T_{\text{kin}} = 10$ K and $n(\text{H}_2) = 10^4 \text{ cm}^{-3}$, and for the outflow, we

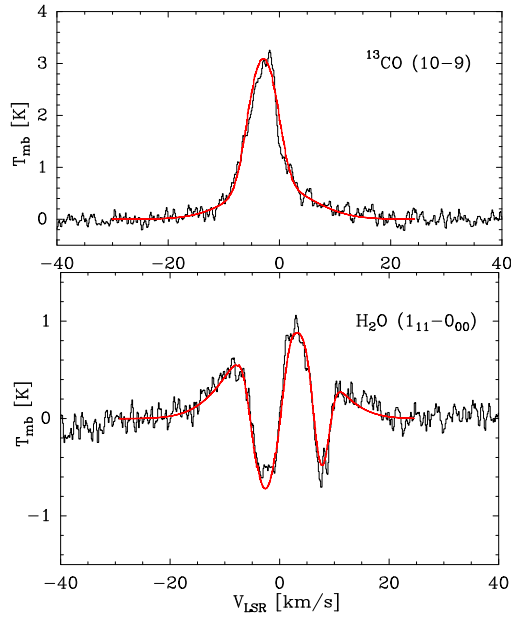


Fig. 4. Data from Fig. 2 with radiative transfer models superposed.

Table 1. Abundances and column densities of ^{13}CO and H_2O .

| Component | $N(^{13}\text{CO})^a$ 10^{16} cm^{-2} | $N(\text{p-H}_2\text{O})$ 10^{12} cm^{-2} | $N(\text{H}_2)$ 10^{21} cm^{-2} | $x(\text{p-H}_2\text{O})$ |
|------------|----------------------------------------------------|--------------------------------------------------------|----------------------------------------------|---------------------------|
| Dense core | 7.8×10^{-7} | ... | ... | 1.6×10^{-10} |
| Outflow | 5 | 10,000 | 15 | 7×10^{-7} |
| Foreground | 0.7 | 4 | 2.1 | 4×10^{-9} |

^a: Abundance for the dense core

adopt $T_{\text{kin}} = 200 \text{ K}$ and $n(\text{H}_2) = 3 \times 10^4 \text{ cm}^{-3}$, which assumptions introduce a factor of ~ 2 uncertainty each. To estimate $N(^{13}\text{CO})$ for the foreground cloud, we use the $J=1-0$ observations by Jakob et al. (2007).

Table 1 summarizes our derived column densities and abundances of ^{13}CO and H_2O in the various physical components of the DR21 region. Our H_2O abundance in the dense core is $\sim 100\times$ lower than previous determinations (§1) but should be regarded as a lower limit. At the low temperatures and high densities in the core, most H_2O is likely frozen on grains, and the observed line may arise in a small region with a high H_2O abundance. The derived ^{13}CO abundance for the core is $\sim 4\times$ lower than expected for the above values of the CO isotopic ratios and abundance, which suggests that even some CO is frozen out in the outer parts of the core. The density of the foreground cloud is too low for significant freeze-out, but with $A_V \approx 1.2 \text{ mag}$, photodissociation is rapid for H_2O but not for ^{13}CO .

The high H_2O abundance for the outflow is likely related to its temperature of $\sim 200 \text{ K}$, which is high enough to have H_2O released from the dust grains by thermal evaporation, or possibly by shocks (Melnick et al. 2008). Further enhancement may be expected in even warmer gas ($\gtrsim 250 \text{ K}$) when neutral-neutral reactions drive most gas-phase oxygen into H_2O , but such gas is not probed by our data. Future HIFI observations of high-excitation H_2O lines towards protostars of all masses will however very likely reveal this effect.

Acknowledgements. HIFI has been designed and built by a consortium of institutes and university departments from across Europe, Canada and the US under

the leadership of SRON Netherlands Institute for Space Research, Groningen, The Netherlands with major contributions from Germany, France and the US. Consortium members are: Canada: CSA, U.Waterloo; France: CESR, LAB, LERMA, IRAM; Germany: KOSMA, MPIfR, MPS; Ireland, NUI Maynooth; Italy: ASI, IFSI-INAF, Arcetri-INAF; Netherlands: SRON, TUD; Poland: CAMK, CBK; Spain: Observatorio Astronómico Nacional (IGN), Centro de Astrobiología (CSIC-INTA); Sweden: Chalmers University of Technology - MC2, RSS & GARD, Onsala Space Observatory, Swedish National Space Board, Stockholm University - Stockholm Observatory; Switzerland: ETH Zürich, FHNW; USA: Caltech, JPL, NHSC.

References

- Ashby, M. L. N., Bergin, E. A., Plume, R., et al. 2000, *ApJ*, 539, L115
 Bjerkeli, P., Liseau, R., Olberg, M., et al. 2009, *A&A*, 507, 1455
 Braz, M. A. & Epchtein, N. 1983, *A&AS*, 54, 167
 Faure, A., Crimier, N., Ceccarelli, C., et al. 2007, *A&A*, 472, 1029
 Flower, D. R. 2001, *Journal of Physics B Atomic Molecular Physics*, 34, 2731
 Garden, R., Hayashi, M., Hasegawa, T., et al. 1991, *ApJ*, 374, 540
 Gibb, A. G., Thompson, M. A., Wyrowski, F., & Hatchell, J. 2005, *P&P V*, 8194
 Hogerheijde, M. R. & van der Tak, F. F. S. 2000, *A&A*, 362, 697
 Jakob, H., Kramer, C., Simon, R., et al. 2007, *A&A*, 461, 999
 Kirby, L. 2009, *ApJ*, 694, 1056
 Lacy, J. H., Knacke, R., Geballe, T. R., & Tokunaga, A. T. 1994, *ApJ*, 428, L69
 Marseille, M., Bontemps, S., Herpin, F., et al. 2008, *A&A*, 488, 579
 Melnick, G. J. & Bergin, E. A. 2005, *Advances in Space Research*, 36, 1027
 Melnick, G. J., Tolls, V., Neufeld, D. A., et al. 2008, *ApJ*, 683, 876
 Milam, S., Savage, C., Brewster, M., et al. 2005, *ApJ*, 634, 1126
 Motte, F., Bontemps, S., Schilke, P., et al. 2007, *A&A*, 476, 1243
 Müller, H., Schlöder, F., Stutzki, J., et al. 2005, *J. Mol. Struct.*, 742, 215
 Ott, J. 2010, *ADASS XIX*, in press
 Poelman, D. R. & van der Tak, F. F. S. 2007, *A&A*, 475, 949
 Roelfsema, P. R., Goss, W. M., & Geballe, T. R. 1989, *A&A*, 222, 247
 Schneider, N., Bontemps, S., Simon, R., et al. 2006, *A&A*, 458, 855
 Van der Tak, F., Black, J., Schöier, F., et al. 2007, *A&A*, 468, 627
 Van der Tak, F., van Dishoeck, E., Evans, II, N., & et al. 2000, *ApJ*, 537, 283
 Van der Tak, F., Walmsley, C., Herpin, F., et al. 2006, *A&A*, 447, 1011
 Van Dishoeck, E. F. & Helmich, F. P. 1996, *A&A*, 315, L177
 Watson, D. M., Bohac, C. J., Hull, C., et al. 2007, *Nature*, 448, 1026
 Wolf, S. & Henning, T. 2000, *Computer Physics Communications*, 132, 166
 Zinnecker, H. & Yorke, H. W. 2007, *ARA&A*, 45, 481

-
- ¹ SRON Netherlands Institute for Space Research, Landleven 12,
9747 AD Groningen, The Netherlands; e-mail: vdtak@sron.nl
 - ² Kapteyn Institute, University of Groningen, The Netherlands
 - ³ Laboratoire d'Astrophysique de Bordeaux, Floirac, France
 - ⁴ Max-Planck-Institut für Radioastronomie, Bonn, Germany
 - ⁵ Sterrewacht, Universiteit Leiden, The Netherlands
 - ⁶ KOSMA, I.Physik.Institut, Universität zu Köln, Germany
 - ⁷ CESR, Université de Toulouse, France
 - ⁸ Chalmers University of Technology, 41296 Göteborg, Sweden
 - ⁹ Institute of Astronomy, ETH Zürich, 8093 Zürich, Switzerland
 - ¹⁰ Joint ALMA Observatory, Santiago, Chile
 - ¹¹ European Space Astronomy Centre, ESA, Madrid, Spain
 - ¹² Harvard-Smithsonian Center for Astrophysics, Cambridge, USA
 - ¹³ Denison University, Granville OH, USA
 - ¹⁴ MPI für Extraterrestrische Physik, Garching, Germany
 - ¹⁵ School of Physics and Astronomy, University of Leeds, UK
 - ¹⁶ Herzberg Institute of Astrophysics, Victoria, Canada
 - ¹⁷ Dept of Physics and Astronomy, University of Victoria, Canada
 - ¹⁸ Observatorio Astronómico Nacional, Alcalá de Henares, Spain
 - ¹⁹ INAF - Istituto di Fisica dello Spazio Interplanetario, Roma, Italy
 - ²⁰ Dept of Astronomy, University of Michigan, Ann Arbor, USA
 - ²¹ California Institute of Technology, Pasadena CA 91125, USA
 - ²² CAB, INTA-CSIC, Torrejón de Ardoz, Spain
 - ²³ University of Amsterdam, The Netherlands
 - ²⁴ LERMA and UMR 8112 du CNRS, Observatoire de Paris, France
 - ²⁵ Dept of Physics and Astronomy, University of Waterloo, Canada
 - ²⁶ Centre for Star and Planet Formation, U. of Copenhagen, Denmark
 - ²⁷ Department of Astronomy, Stockholm University, Sweden
 - ²⁸ Johns Hopkins University, Baltimore, USA
 - ²⁹ JPL, California Institute of Technology, Pasadena, CA 91109, USA
 - ³⁰ Dept of Physics and Astronomy, University of Calgary, Canada
 - ³¹ Observatoire de Paris-Meudon, Meudon, France